October 4, 2017

First-Principles and Model Simulation of All-Optical Spin Reversal

Thomas F George, *University of Missouri-St. Louis*
G.P. Zhang, *Indiana State University*
Z. Babyak
Y. Xue
Y. H. Bai

First-principles and model simulation of all-optical spin reversal

G. P. Zhang, Z. Babyak, and Y. Xue
Department of Physics, Indiana State University, Terre Haute, Indiana 47809, USA

Y. H. Bai
Office of Information Technology, Indiana State University, Terre Haute, Indiana 47809, USA

Thomas F. George
Office of the Chancellor and Center for Nanoscience, Department of Chemistry and Biochemistry, and Department of Physics and Astronomy, University of Missouri–St. Louis, St. Louis, Missouri 63121, USA

(Received 1 May 2017; revised manuscript received 5 September 2017; published 4 October 2017)

All-optical spin switching is a potential trailblazer for information storage and communication at an unprecedented fast rate free of magnetic fields. However, the current wisdom is largely based on semiempirical models of effective magnetic fields and heat pulses, so it is difficult to provide high-speed design protocols for actual devices. Here, we carry out a massively parallel first-principles and model calculation for 13 spin systems and magnetic layers, free of any effective field, to establish a simpler and alternative paradigm of laser-induced ultrafast spin reversal and to point out a path to a full-integrated photospintronic device. It is the interplay of the optical selection rule and sublattice spin orderings that underlines seemingly irreconcilable helicity-dependent and -independent switchings. Using realistic experimental parameters, we predict that strong ferrimagnets, in particular, Laves phase C15 rare-earth alloys, meet the telecommunication energy requirement of 10 fJ, thus allowing a cost-effective subpicosecond laser to switch spin in the gigahertz region.

DOI: 10.1103/PhysRevB.96.134407

I. INTRODUCTION

Advanced material engineering and ultrafast laser technology revolutionize the way that information is stored and transmitted [1]. Over a half century, switching magnetic moments exclusively relied on magnetic fields, but now multiferroics allows the electric field to control spins [2]. Spins can also be manipulated by correlated spin-charge quantum excitations [3] and intense terahertz transients [4–7]. Spin-orbit coupling adds a new dimension to control spin currents [8]. Very recently, 55-fs spin canting in Fe nanoparticles was discovered [9]. Remarkably, a single laser pulse is capable of switching a quantum spin from one orientation to another [10], free of a magnetic field. This all-optical spin switching (AOS) immediately ignited the entire community of ultrafast magnetic storage and information communication [11–15], but results are much more complex. The switching in ferrimagnetic GdFeCo was found to be helicity dependent [10], but when the laser fluence was above a particular threshold, helicity-dependent spin switching (HDS) transitions to helicity-independent switching (HIDS) [16]. However, such a transition is not seen in other ferrimagnets [12–14,17] or in ferromagnets [18]. A stronger laser does not lead to HIDS and only demagnetizes the sample. These paradoxically contradictory results challenge our understanding and are difficult to reconcile. Over the years, the explanation progressed from the inverse Faraday effect [10,19], Raman scattering [20,21], magnetic circular dichroism [22], pure heating [16], and sublattice spin exchange [23] to ultrafast exchange scattering [24], with new theories emerging in ferromagnets [25–27]. This raises a serious question about whether a big picture is missing from the existing theories [28]. Furthermore, no theory ever addressed a design protocol for future photospintronic devices based on AOS technology [29].

In this paper, we establish an alternative and simpler paradigm for laser-induced all-optical spin reversal and establish a path to future applications. We carry out an extensive time-dependent first-principles and model calculation for 13 carefully selected spin and layer systems. Different from prior studies, our theory does not invoke an effective magnetic field or a heat pulse, thus reflecting the experimental situation better. We show that the helicity-dependent AOS is the manifestation of the optical selection rule, a finding that is corroborated by the first-principles results. Sublattice spins provide additional degrees of freedom to control spin reversal. However, for a weak ferrimagnet, the selection rule is still operative, so the switching is helicity dependent. A sudden change occurs in a strong ferrimagnet, where the sublattice spins differ a little in their magnitude and switching becomes helicity independent. We construct a phase diagram for the entire spin reversal. Using the experimental parameters [30], we show that in the strong ferrimagnet limit, the energy consumption is already below the technological requirements. We find that Laves phase C15 rare-earth alloys are ideal candidates for future spin switching in the gigahertz region.

II. THEORETICAL FORMALISM

There are several attractive theories available, but most of them introduce an effective magnetic field or a heat pulse, whereas, experimentally, no magnetic field is applied. We see that there is room for improvement. We employ two complementary theories: one is the first-principles method, and the other is a model simulation. Such a joint study is necessary, as seen below, in that it allows us to flexibly investigate different aspects of all-optical spin reversal and cross-check the results, so we can develop a simple and more complete picture for AOS. Different from prior theories, none

of our theories need either an effective magnetic field or a heat pulse. So our theories are closer to the experimental reality and present an alternative to existing theories which are based on the Landau-Lifshitz-Gilbert-Bloch formalism. We draw connections with those prior theories whenever possible.

A. Time-dependent first-principles calculation

In our first-principles studies, we first solve the Kohn-Sham equation (in atomic units) self-consistently,

$$\left[-\nabla^2 + V_{Ne} + V_{ee} + V_{xc}^{\sigma}\right]\psi_{nk}(r) = E_{nk}\psi_{nk}(r). \quad (1)$$

where the terms on the left side are kinetic energy, electron-nuclear attraction energy, and Coulomb and exchange correlations, respectively. $\psi_{nk}(r)$ and E_{nk} are the eigenstates and eigenenergies at the k point for band n. We use the full-potential augmented plane-wave method as implemented in the WIEN2K code [31], where the spin-orbit coupling is also included. The dynamic simulation starts with the Liouville equation,

$$i\hbar\frac{\partial\rho}{\partial t} = [H_0 + H_I, \rho], \quad (2)$$

where ρ is the density matrix and H_0 is the unperturbed system Hamiltonian. H_I is the interaction between the system and laser field: $H_I = \sum_{k;i,j}\mathbf{P}_{k;i,j}\cdot\mathbf{A}(t)$, where $\mathbf{P}_{k;i,j}$ is the momentum matrix element between states i and j at k and $\mathbf{A}$ is the vector potential with amplitude A_0. For all the first-principles calculations below, we use the vector field potential amplitude A_0 in units of V fs/Å. Once we solve the Liouville equation, we compute the spin expectation value by the trace $\mathrm{Tr}(\rho S_z)$.

B. Model simulation

In our model simulation, we adopt a thin slab, with two monolayers along the z axis and 21 lattice sites along the x and y axes. Spins are orderly arranged in a simple cubic structure, thus removing any ambiguity in spin configuration. We verify that our system is large enough that the finite-size effect is small. When we construct our model, we are mindful that it cannot include every detail in a sample; otherwise, the problem would become intractable. With this in mind, we construct our model Hamiltonian as [28,32,33]

$$H = \sum_i\left[\frac{\mathbf{p}_i^2}{2m} + V(\mathbf{r}_i) + \lambda\mathbf{L}_i\cdot\mathbf{S}_i - e\mathbf{E}(t)\cdot\mathbf{r}_i\right] - \sum_{ij}J_{ex}\mathbf{S}_i\cdot\mathbf{S}_j, \quad (3)$$

where the terms on the right side are the kinetic energy, potential energy, spin-orbit coupling, interaction between the laser field and the system, and the Heisenberg exchange interaction between the nearest-neighbor sites. A similar form is often used for magnetic multilayers [34,35]. $\mathbf{L}_i$ and $\mathbf{S}_i$ are orbital and spin angular momenta at site i, respectively, and J_{ex} is the exchange integral in units of $\mathrm{eV}/\hbar^2$. Since each site contains one spin, as a standard practice, we use the same index i to denote both the spin and atomic site. The nearest-neighbor spins are coupled either antiferromagnetically or ferromagnetically. Ferrimagnets have two sublattices, S_z^a and S_z^b.

Our model contains four minimum conditions for spin reversal: (i) a channel for the laser to transfer the energy and angular momentum into the system, (ii) a transient increase of the orbital angular momentum [36], (iii) emergent spin-orbit torque [33], and (iv) spin-spin interaction [16]. One can show easily that with any one of them missing, spin switching founders. To make connections with prior theories, we should point out that the inverse Faraday effect [10] is intrinsically connected to the spin-orbit coupling in Eq. (3), and both Raman scattering [20,21] and magnetic circularly dichroism [22] are included through the first four terms in the equation, while the sublattice exchange interaction [23] and scattering [24] are included in the last term of the equation. Ostler *et al.* [16] essentially replaced the first three terms by a phenomenological heat pulse. The major difference between our work and Ref. [21] is that they worked with the wave function, so the spin-orbit torque was hidden behind the convoluted wave function. In our theory, we work with operators directly, so it is easier to reveal the role of the spin-orbit torque in spin reversal. Our theory [32] also recovers the results by Pershan *et al.* [37]. Spin-orbit torque is also similar to the spin-orbit-induced torque by Manchon and Zhang [35]. The only difference is that their driving field was current and, in our case, we have a laser field. Our Hamiltonian is a quantum-mechanical many-body Hamiltonian. Such a model is difficult to solve exactly, and approximations have to be made.

We solve Heisenberg's equation of motion numerically for each operator of interest under the influence of a laser field within the Hartree-Fock approximation. The validity of this approximation is checked by comparing our results with the experimental ones. The exchange interaction is $J_{ex} = 0.1\mathrm{eV}/\hbar^2$, and the laser pulse duration is $\tau = 240$ fs.

III. RESULTS AND DISCUSSIONS

A. Optical selection rule

To start with, we note that all-optical spin reversal is an optical process and must follow the dipole selection rule. Consider a laser field propagating along the $-z$ axis toward a sample surface [28,32] (see Fig. 1),

$$\mathbf{E}(t) = E_0 e^{-t^2/\tau^2}[\pm\sin(\omega t)\hat{x} + \cos(\omega t)\hat{y}], \quad (4)$$

where E_0 is the laser field amplitude (in units of V/Å; not to be confused with the vector potential A_0 above), ω is the carrier frequency, τ is the laser pulse duration, and $\hat{x}$ and $\hat{y}$ are the unit vectors along the x and y directions, respectively. The $+$ $(-)$ sign refers to right- (left-) circularly polarized light $\sigma^{+(-)}$. In atoms, any spin states are characterized by the total angular momentum quantum number J in the presence of spin-orbit coupling; in solids, the rule is still there but manifests itself through the optical transition matrix elements at every crystal momentum point in the reciprocal space. For right- and left-circularly polarized light σ^+ and σ^-, J changes as [38]

$$\Delta J = \begin{cases} +1(\sigma^+) & \uparrow\Longrightarrow\downarrow, \\ -1(\sigma^-) & \downarrow\Longrightarrow\uparrow, \end{cases} \quad (5)$$

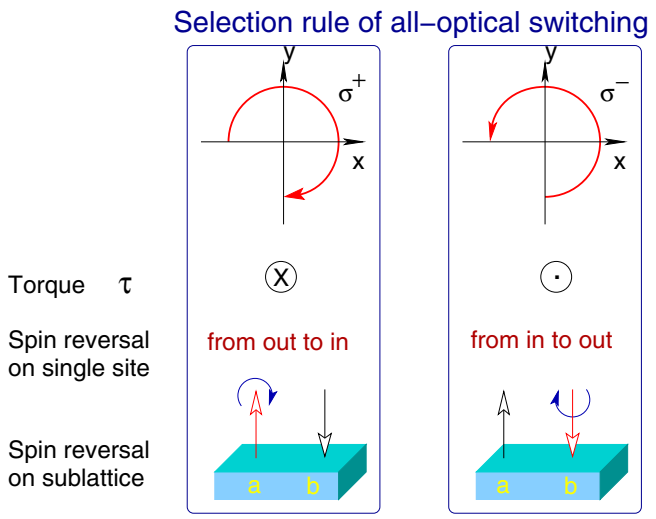

FIG. 1. Selection rule for all-optical spin switching. The light helicity determines the direction of the spin-orbit torque τ. Left: For a single spin, right-circularly polarized light σ^+ rotates the spin from out of the page into the page. Right: σ^- light does the opposite. Bottom: For a system with two sublattices a and b, σ^- and σ^+ switch different sets of spins. σ^+ switches a spin from up to down, while σ^- switches a spin from down to up.

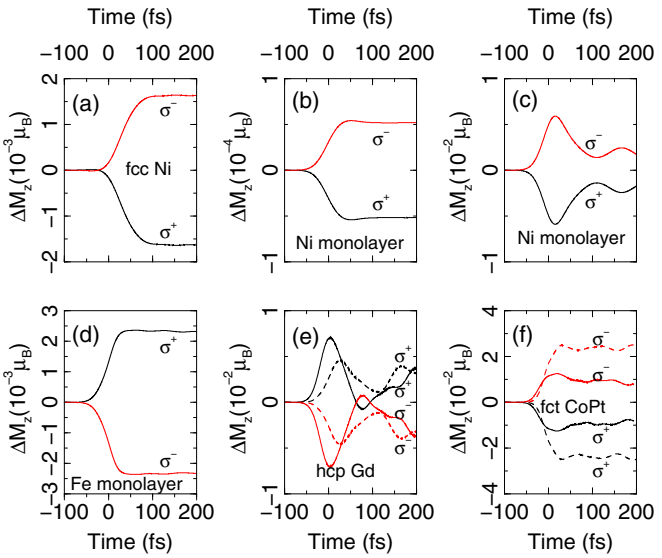

FIG. 2. First-principles simulation of helicity-dependent spin moment change ΔM_z for (a) fcc Ni, (b) and (c) a Ni free-standing monolayer, (d) an Fe monolayer, (e) hcp Gd, and (f) fct CoPt. $\Delta M_z^{\sigma^\pm} = M_z^{\sigma^\pm} - (M_z^{\sigma^+} + M_z^{\sigma^-})/2$. Here, $M_z^{\sigma^{+/-}}$ is the spin moment under $\sigma^{+/-}$ excitation. Laser parameters are as follows. (a) Duration $\tau = 60$ fs, photon energy $\hbar\omega = 2.0$ eV, and vector potential amplitude $A_0 = 0.0099$ V fs/Å. (b) $\tau = 48$ fs, $\hbar\omega = 1.6$ eV, and $A_0 = 0.0030$ V fs/Å. (c) $\tau = 48$ fs, $\hbar\omega = 1.55$ eV, and $A_0 = 0.030$ V fs/Å. (d) $\tau = 48$ fs, $\hbar\omega = 2.0$ eV, and $A_0 = 0.030$ V fs/Å. (e) Solid line: $\tau = 48$ fs, $\hbar\omega = 1.6$ eV, and $A_0 = 0.030$ V fs/Å; dashed line: $\tau = 48$ fs, $\hbar\omega = 1.55$ eV, and $A_0 = 0.030$ V fs/Å. (f) Solid line: $\tau = 48$ fs, $\hbar\omega = 1.6$ eV, and $A_0 = 0.030$ V fs/Å; dashed line: $\tau = 48$ fs, $\hbar\omega = 1.55$ eV, and $A_0 = 0.030$ V fs/Å.

where the double-line arrows emphasize the angular momentum passage between the spin and orbital degrees of freedom.

To visualize how the spin reversal happens, Fig. 1 illustrates the helicity dependence of spin reversal in the x-y plane. On the left side of the figure, we have right-circularly polarized light, where the electric field rotates clockwise and its induced spin-orbit torque $\tau_{\rm soc}$ [33] follows the normal right-hand rule. If we curl our fingers along the light helicity direction, the thumb points in the direction of the torque. In this case, it points into the page. If the original spin points out of the page, under the influence of this torque, it will be reversed into the page. But if the spin already points into the page, then there is no effect on this spin. If we choose left-circularly polarized light (see the right side of Fig. 1), the situation is reversed, and $\tau_{\rm soc}$ points out of page. This rule is very powerful and allows us to figure out how the spin reverses. The bottom panel shows that the thin film has two spin sublattices, a and b. Suppose the spin on a points out of the plane of the film and that on b into the plane. If the σ^+ laser comes down on the film, only the sublattice spin a (in red) is affected. The effect on sublattice spin b is through the exchange interaction. If we use σ^-, then the spin on sublattice b is affected. However, the selection rule provides only a possibility to switch spins and cannot give a definitive answer to whether the reversal actually occurs. This requires a first-principles calculation.

B. Time-dependent Liouville density-functional study of helicity dependence

Chimata *et al.* [39] employed the first-principles method, but their switching in Gd-Fe alloys was simulated via a model [16]. Another approach also appeared [40], where the calculation was static. Time-dependent density-functional theory (DFT) has been employed to investigate an ultrafast demagnetization field [41–44] but not for spin reversal. We carry out an extensive density-functional calculation and time-dependent Liouville simulation [45] under circularly polarized light. This method slightly differs from the traditional time-dependent density-functional theory, where our time propagation is done through the Liouville equation and electron excitation is described by the density matrix. We employ three element ferromagnets (Ni, Fe, and Gd) and one alloy (CoPt), with different structures (fcc, fct, hcp, and monolayer) and four sets of laser parameters with left- and right-circular polarizations, together with eight Laves phase (C15) rare-earth intermetallic compounds (see below). The details of the structural and magnetic information are given in the Supplemental Material [46].

The calculations consist of two steps: (i) self-consistent DFT calculation with the WIEN2K code [31] and (ii) solving the time-dependent Liouville equation. Since the helicity dependence of spin reversal is always superimposed on the demagnetization (see details in the Supplemental Material [46]), we subtract the average spin moment $\bar{M}_z = (M_z^{\sigma^+} + M_z^{\sigma^-})/2$ from the moment for each helicity to get the net effect of the helicity dependence, $\Delta M_z^{\sigma^\pm} = M_z^{\sigma^\pm} - \bar{M}_z$. Here, $M_z^{\sigma^{+/-}}$ is the spin moment under $\sigma^{+/-}$ excitation.

Figure 2(a) shows that σ^+ and σ^- have different effects on the moment in fcc Ni, and σ^+ reduces the moment more, which can be understood from the above dipole selection rule. Such

a helicity dependence is also observed in a Ni free-standing monolayer [see Fig. 2(b)]. If we increase the field amplitude by 10 times, the moment change becomes oscillatory for σ^+ and σ^- [see Fig. 2(c)], and the net change in moment increases 100 times, but the relative moment change for σ^+ and σ^- remains the same.

However, this is no longer the case for an Fe monolayer, where σ^- decreases the moment more than σ^+ [see Fig. 2(d)]. This is because only those pockets in the k space that are optically accessible can contribute to the moment change, and the global moment direction may not align with the local moment direction.

Hexagonal-close-packed Gd is particularly interesting. The solid line in Fig. 2(e) shows that σ^- induces a larger change, but around 75 fs, σ^+ has a larger change. If we reduce the photon energy to 1.55 eV, such a crossover is not seen [see the dashed lines in Fig. 2(e)]. We did not find a similar case in other materials investigated.

Face-centered tetragonal CoPt is very unique and has a strong magnetic anisotropy. Its moment change [Fig. 2(f)] is larger than others under a similar laser excitation and increases twice if we use a 1.55 eV pulse instead of 1.60 eV. This reflects the importance of the laser photon energy. In summary, our first-principles result unambiguously demonstrates that the helicity dependence of the moment dynamics is generic, but the degree of the helicity effect is very much material dependent.

C. Impact of sublattice spins on spin reversal

While our first-principles investigation lays the ground work for spin reversal, it cannot fine-tune its sublattice spins at each lattice and gives no direct information about the effect of sublattice spin ordering on spin reversal. Our model, with a realistic laser pulse, provides complementary information. We investigate three representative spin systems, a ferromagnet (FM) and weak and strong ferrimagnets (FIMs), to approximately simulate ferromagnets [17,18], TbCo alloys [13,15], and, to some extent, GdFeCo alloys [10], respectively. We emphasize that all the calculations below use the same sample geometry ($21 \times 21 \times 2$) and parameters, and we change only the sublattice spins, so their impact on spin reversal can be investigated unambiguously.

Figure 3 shows a comprehensive view of how the spin reversal depends on the laser field amplitude E_0 as the spin ordering changes from a ferromagnetic to a weak and then strong ferrimagnetic phase. Figure 3(a) shows that the ferromagnetic layer, with a single sublattice spin $S_z^a = S_z^b = 1\hbar$, has a pronounced helicity dependence. With the initial spin up, only σ^+ is effective, and σ^- has virtually little effect, fully consistent with the selection rule discussed above and the experimental findings [18].

The situation is different when the system has two spin sublattices. As seen in Fig. 1, when both spin orientations are present, σ^+ and σ^- excite different sets of spins. We retain the spin on sublattice a but flip and reduce the spin on sublattice b by half to $S_z^b = -0.5\hbar$, which we call a weak ferrimagnet, thus mimicking TbCo alloys. We note in passing that these spin angular momenta are chosen as examples and have no effect on our conclusion qualitatively, as far as they satisfy the minimum momentum requirement [33]. Figure 3(b) shows that

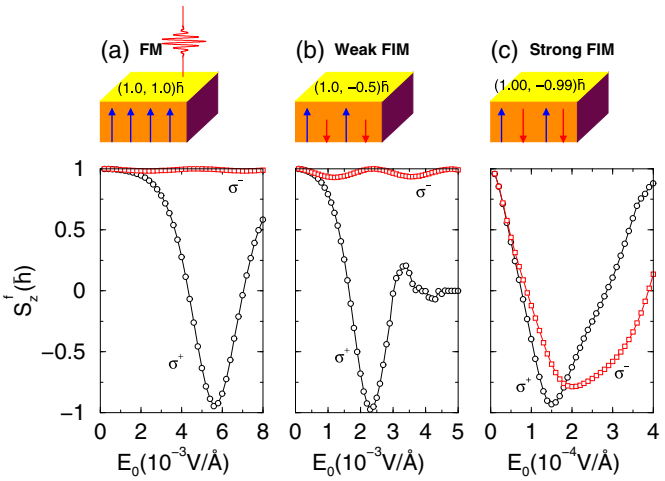

FIG. 3. Dependence of the final spin angular momentum on the laser field amplitude E_0 under right- and left-circularly polarized light in a (a) ferromagnet, (b) weak ferrimagnet, and (c) strong ferrimagnet. $\tau = 240$ fs. The open circles denote the results with σ^+, and the open squares denote those with σ^-. The optimal amplitudes for σ^+ (σ^-) reduce from (a) 0.0056 0.0024) V/Å to (b) 0.0023 (0.0012) V/Å to (c) 0.00015 (0.0002) V/Å.

σ^+ is capable of reversing the spin from $1.0\hbar$ to $-0.98\hbar$ (see the open circles), with nearly 100% switchability, even with a smaller optimal field amplitude of 2.3×10^{-3} V/Å than the value of 5.6×10^{-3} V/Å in the FM case. In contrast to the FM, down spins on sublattice b of the FIM, which are not supposed to directly flip under σ^+ according to Fig. 1, are also switched over but *indirectly through the exchange interaction* J_{ex}. This means that unlike the FM, the FIM has two channels to switch spins, either directly through *correct* light helicity or indirectly through the exchange interaction. σ^- also affects the spins, and there is a clear modulation in the spin with the field amplitude [see the open squares in Fig. 3(b)], but σ^- is still much less effective. This reveals the crucial insight that if the sublattice spin magnitudes differ a lot, only one helicity can reverse spins effectively, so the switching remains highly helicity dependent. We believe that this is what happens in ferrimagnetic TbCo. Its sublattice effective spin on Tb is much larger than that on Co. Here, the effective spin must be used since TbCo alloys have different concentrations [28,33].

So far, all the switchings have been helicity dependent. To understand HIDS, we need to understand the magnetic structure difference between GdFeCo and TbCo alloys. Fe has a larger spin moment than Co, so the effective spin difference between Gd and Fe sites in GdFeCo is much smaller than that between Tb and Co in TbCo. In fact, GdFeCo alloys have nearly compensated spins on two sublattices. Hassdenteufel *et al.* [15] even proposed the low remanence as a criterion for AOS. Our strong ferrimagnet model simulates such a scenario where the spin on sublattice b is only 1% smaller than the spin on sublattice a, i.e., $S_z^a = 1\hbar$ and $S_z^b = -0.99\hbar$ [see Fig. 3(c)]. The system is very close to an antiferromagnet. Figure 3(c) shows that both σ^+ and σ^- are effective to switch spin, thus realizing a helicity-independent switching. σ^- induces a final average spin of $-0.79\hbar$ at the optimal field amplitude.

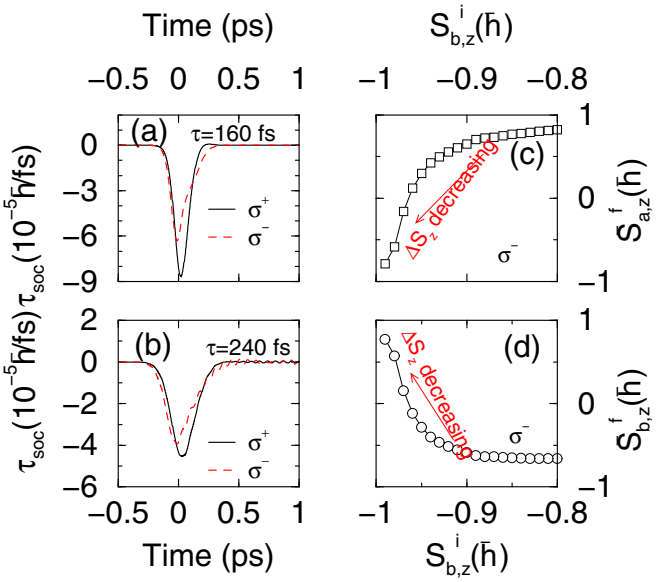

FIG. 4. (a) Laser-induced spin-orbit torque τ_{soc} as a function of time for σ^+ (solid line) and σ^- (dashed line) pulses; $\tau = 160$ fs. (b) Same as (a), but $\tau = 240$ fs. (c) Final average spin at sublattice a as a function of the initial spin on sublattice lattice b. ΔS_z is the sublattice spin magnitude difference. (d) Final average spin at sublattice b as a function of the initial spin on sublattice lattice b.

The importance of sublattice spins has long been recognized [23], but the interplay between the sublattice spin and light helicity has not. In Fig. 4 we explain why σ^+ appears more powerful to reverse spins than σ^-. Figure 4(a) shows the time evolution of optical spin-orbit torques (OSOT) [33] for σ^+ (solid line) and σ^- (dashed line) pulses. The electric field in Eq. (4) first excites the orbital angular momentum [28] and then OSOT. The definition of OSOT is $\tau_{soc} = \lambda \mathbf{L} \times \mathbf{S}$. It is clear that OSOT critically depends on the magnitude of the spin (compare the solid and dashed lines), and the spin evolution contains both precession and flipping. Since the down spin has a smaller magnitude, its torque is smaller, so the switching under σ^- excitation is not as perfect as that under σ^+. Increasing the pulse duration from $\tau = 160$ to 240 fs [Fig. 4(b)] reduces the torque difference between σ^+ and σ^-. These torques are the time-dependent analog of the effective magnetic field introduced in the inverse Faraday effect (IFE) [10], but IFE has never been formulated in terms of light helicity and spin and orbital angular momenta [21], so it is unable to draw the crucial connection to AOS. Our finding establishes an important paradigm that sublattice spins directly impact how the helicity switches spins, being helicity dependent or helicity independent. The key is that the spin-orbit torque τ_{soc} intrinsically depends on the magnitude of the spin; thus, the helicity dependence of AOS becomes spin dependent. Figure 4(c) shows that as $S^i_{b,z}$ decreases from $-0.8\hbar$ to $-0.9\hbar$, the final spin on sublattice a, $\bar{S}^f_{a,z}$, has a very small decrease, but once $S^i_{b,z}$ is below $-0.95\hbar$ or ΔS_z is below $0.05\hbar$, $\bar{S}^f_{a,z}$ decreases superlinearly and reaches $-0.79\hbar$. The results for sublattice b are plotted in Fig. 4(d). We see similarly that as ΔS_z decreases, $\bar{S}^f_{b,z}$ increases superlinearly.

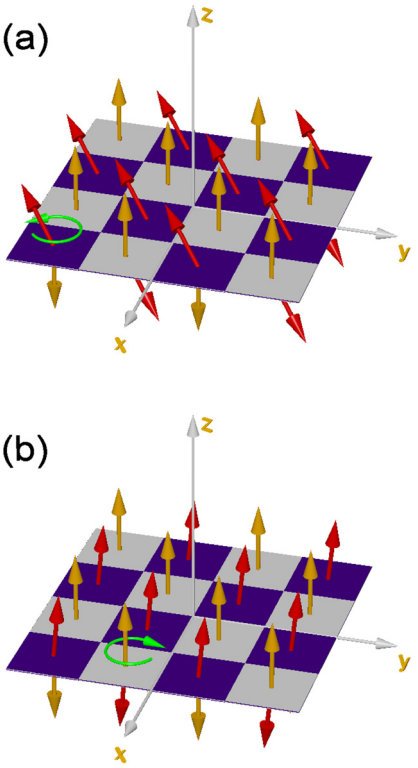

FIG. 5. (a) Snapshot of spins at the center of a strong ferrimagnet before (gold arrows) and 2 ps after (red arrows) σ^- excitation. A partial reversal is observed. The torus arrow shows which spins the laser initially switches. (b) Snapshot of spins at the center of the slab before (gold arrows) and 2 ps after (red arrows) σ^+ excitation. A nearly complete reversal is found. The torus arrow shows which spins the laser initially switches.

D. Snapshot of spin reversal

So far we have shown the spin dynamics of one representative spin. Now we show a group of spins at the center part of the first layer. The gold arrows in Fig. 5(a) are the initial spins on two sublattices. They take values of $+1\hbar$ and $-0.99\hbar$ and form a ferrimagnetic network extending along all three directions. The red arrows in Fig. 5(a) capture a snapshot of the spins at 2 ps after σ^- excitation. Spins in the second layer are similar (not shown). We see that all the spins, regardless of their original orientations, are reversed or, more precisely, cant toward opposite directions. The green torus arrow highlights that a σ^- pulse selectively switches those down spins up first and then those initial up spins through the exchange interaction. Figure 5(b) shows that the switching with σ^+ is nearly perfect, with all the spins pointing in the opposite directions of the initial spins. The green torus arrow shows another example in which a σ^+ pulse selectively switches the up spins first. If the gray squares in Fig. 5(a) represent spin up and the blue ones represent spin down, σ^- and σ^+ are going to reverse those domains selectively.

The entire process is pretty much similar to the superresolved fluorescence microscopy which was recognized by the Nobel Prize in Chemistry in 2014, where fluorescent proteins act as an agent to beat the diffraction limit. In our case, the agent is the magnetic domain. These magnetic domains allow

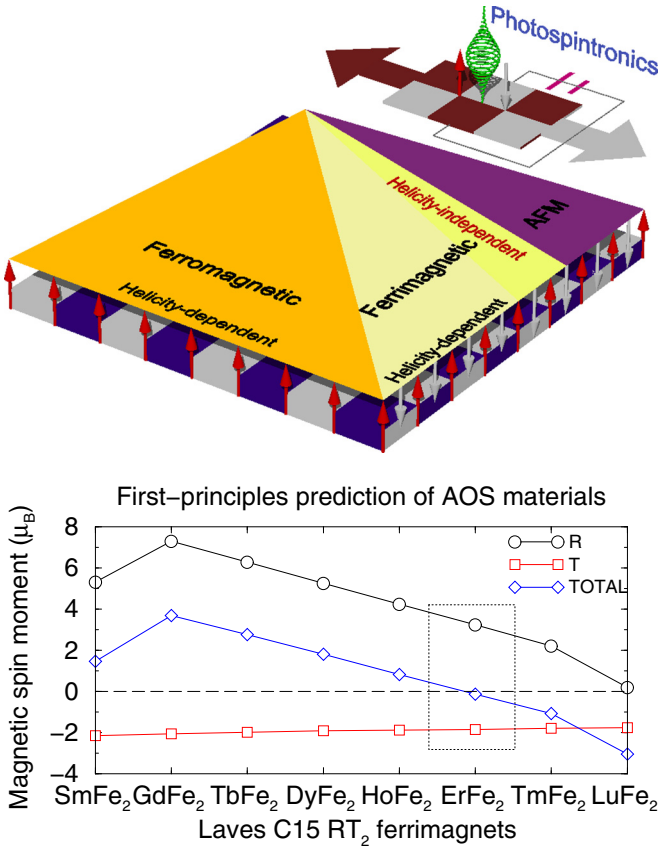

FIG. 6. Top left: Phase diagram of AOS. Switchings in the FM (orange triangle) and weak FIM (light yellow triangle) are always helicity dependent. Helicity-independent switching (dark yellow triangle) occurs in a narrow region when the sublattice spins approach the antiferromagnetic limit. Top right: The envisioned photospintronic device is based on a strong ferrimagnet which allows the laser to store and switch spins rapidly. Bottom: Magnetic spin moment for eight Laves phase C15 rare-earth-transition-metal ferrimagnets. The spin moment at the Fe site is almost constant, but that at the R site peaks at $GdFe_2$ and decreases along the series. Around $ErFe_2$, there is an optimal strong ferrimagnetic configuration (dashed box) where an ideal spin reversal may appear. The dashed line is at $0\mu_B$.

subwavelength imaging, which may explain ultrafine magnetic domains created in experiments [17]. Our above finding also explains why experimentally El Hadri *et al.* [47] found that σ^+ (σ^-) switches the magnetization to down (up). In their Co-dominated TbCo alloy films, the spins at Co sites point up initially, while in Tb-dominated films, the spins are down. These two different experiments beautifully demonstrate how accurate our prediction is.

E. Phase diagram

Based on the above results, we construct a phase diagram for AOS in Fig. 6. The essence of this phase diagram is that all the AOS materials should be classified into three types: ferromagnets, weak ferrimagnets, and strong ferrimagnets. On the left, we show that AOS in ferromagnets such as CoPt [18] is always helicity dependent (see the orange triangle). AOS in ferrimagnets (the light yellow triangle) such as TbCo [11], where the sublattice spins differ a lot, is also helicity dependent. A sudden change occurs when the sublattice spins differ very little from each other in strong ferrimagnets such as GdFeCo, just before they become antiferromagnetic. Regardless of laser helicity, the switching is possible for both helicities. The dark yellow triangle denotes this region. This phase diagram not only unifies paradoxically different switching theories into two simple concepts (the optical selection rule and the sublattice spin difference) but also suggests a practical protocol for experimentalists.

TABLE I. Dependence of spin switching on the laser pulse duration in a ferrimagnetic ordered slab under σ^+ pulse excitation. The system size is $21 \times 21 \times 2$. Spins on sublattices a and b are $1\hbar$ and $-0.99\hbar$, respectively. The exchange interaction is 0.1 eV/$\hbar^2$. $E_{\rm opt}$ denotes the optimal laser field amplitude, and $\bar{S}^f$ is the final time-averaged spin at sublattice a. δ is the peak-to-peak amplitude. The spin reversal time T_r is defined as when the spin reaches its first minimum.

τ (fs)	$E_{\rm opt}$ (V/Å)	$\bar{S}^f(\hbar)$	$\delta(\hbar)$	T_r (fs)
160	2.9×10^{-4}	−0.82	0.36	218.09
200	2.0×10^{-4}	−0.90	0.20	305.33
240	1.5×10^{-4}	−0.93	0.14	392.57
360	0.9×10^{-4}	−0.94	0.10	544.42
480	0.7×10^{-4}	−0.95	0.07	609.04

Since an expensive sub-100-fs laser would limit the wide application of AOS, we also examine whether a longer pulse can switch spins as well. Table I shows that as τ increases from 160 to 480 fs [30], the optimal amplitude is significantly reduced as expected. What is even better is that the switching becomes more robust, with a more negative final spin and a much smaller peak-to-peak amplitude δ. This points out an effective path to integrate the ultrafast magnetic storage into rapid optical switching for communication by using stronger ferrimagnets and reasonably longer laser pulses. In 2016, Peregrine Semiconductor Corporation announced 60-GHz switches and with 8-ns switching time [48]. Here, we see that in the strong ferrimagnet pumped with a 480-fs pulse, the spin-reversal time T_r is 609 fs, or 1.6 GHz, thus easily beating the above record. In the top right of Fig. 6, we envision an integrated photospintronic device, where an ultrafast circularly polarized laser pulse stores magnetic bits into a ferrimagnet and the medium controls the signal switching. The signal can be picked up through electric circuits.

IV. FUTURE APPLICATIONS

The state-of-the-art energy consumption for telecommunications is 10 fJ [29]. Figures 3(a) through 3(c) show that for the same laser parameter, a FM needs a much stronger field on the order of 10^{-3} V/Å $\propto 10$ MW/cm^2, but the power drops to 0.1 MW/cm^2 in strong FIMs [see Fig. 3(c)]. We use the experimental parameters from Chen *et al.* [30] and find that the energy consumption is 0.3 fJ. This already meets the requirement of telecommunications switching [29]. Therefore, tailoring the FIM toward an even stronger FIM is likely to accelerate the deployment of AOS-based switching technology.

We can move one step further to suggest some new candidates for AOS. The bottom of Fig. 6 shows the computed spin moments on each rare-earth side and Fe for eight Laves phase C15 phase alloys (RT_2) from $SmFe_2$ through $LuFe_2$ (the details of the calculation are presented in the Supplemental Material [46]). We see that early in the lanthanide series the spin moment on R is much larger than Fe and peaks at $GdFe_2$. This explains why in amorphous GdFeCo the concentration of Gd must be low. However, as in the latter part of the series, the spin moment decreases, so crystalline RT_2 becomes a strong ferrimagnet. A dashed box around $ErFe_2$ highlights such a case. Experimentally, growing these materials has gained renewed interest [49,50]. It is our belief that our finding will further motivate and ignite intense research on photospintronic applications.

V. CONCLUSIONS

We have carried out joint time-dependent first-principles and model calculations to pin down an alternative origin in 13 different magnetic systems. Our results show that all-optical spin switchings can be unified under two crucial concepts: the optical selection rule and the sublattice spin difference. The selection rule dictates that left- (right-) circularly polarized light switches the spin only from down (up) to up (down). This one-to-one correspondence between spin orientation and light helicity is generic, as confirmed by our first-principles results. We constructed a phase diagram to categorize all the magnetic materials into three categories. In ferromagnets, only one spin orientation is present, so they show a strong helicity-dependent switching. For ferrimagnets, we need the second concept, sublattice spin difference. For weak ferrimagnets, with very different sublattice spins, the switching is also helicity dependent. For strong ferrimagnets, with similar sublattice spins, the switching becomes helicity independent, and both σ^+ and σ^- can reverse spins. This conclusion is independent of the system size and exchange interaction and is fundamental to AOS. This represents a paradigm shift for AOS and may have a far-reaching impact on the future of fast magnetic storage technology. We computed the energy consumption in those optimal ferrimagnets and find that it already meets the requirements of the current technology. We have further studied a group of Laves phase C15 rare-earth alloys and have found that their spin moments are ideal for real devices. We expect that our results will motivate further investigations into the laser-induced spin reversal.

ACKNOWLEDGMENTS

We would like to thank Dr. J. Y. Chen, Dr. J. P. Wang, and Dr. M. Li of the University of Minnesota for helpful discussions. This work was solely supported by the U.S. Department of Energy under Contract No. DE-FG02-06ER46304. Part of the work was done on Indiana State University's quantum cluster and high-performance computers. The research used resources of the National Energy Research Scientific Computing Center, which is supported by the Office of Science of the U.S. Department of Energy under Contract No. DE-AC02-05CH11231.

[1] S. D. Bader and S. S. P. Parkin, Spintronics, Annu. Rev. Condens. Matter Phys. **1**, 71 (2010).

[2] J. A. Mundy, C. M. Brooks, M. E. Holtz, J. A. Moyer, H. Das, A. F. Rébola, J. T. Heron, J. D. Clarkson, S. M. Disseler, Z. Liu, A. Farhan, R. Held, R. Hovden, E. Padgett, Q. Mao, H. Paik, R. Misra, L. F. Kourkoutis, E. Arenholz, A. Scholl, J. A. Borchers, W. D. Ratcliff, R. Ramesh, C. J. Fennie, P. Schiffer, D. A. Muller and D. G. Schlom, Atomically engineered ferroic layers yield a room-temperature magnetoelectric multiferroic, Nature (London) **537**, 523 (2016).

[3] T. Li, A. Patz, L. Mouchliadis, J. Yan, T. A. Lograsso, I. E. Perakis, and J. Wang, Femtosecond switching of magnetism via strongly correlated spin-charge quantum excitations, Nature (London) **496**, 69 (2013).

[4] T. Kampfrath, A. Sell, G. Klatt, A. Pashkin, S. Mährlein, T. Dekorsy, M. Wolf, M. Fiebig, A. Leitenstorfer, and R. Huber, Coherent terahertz control of antiferromagnetic spin waves, Nat. Photonics **5**, 31 (2011).

[5] T. Kampfrath, K. Tanaka, and K. A. Nelson, Resonant and nonresonant control over matter and light by intense terahertz transients, Nat. Photonics **7**, 680 (2013).

[6] T. Kubacka, J. A. Johnson, M. C. Hoffmann, C. Vicario, S. de Jong, P. Beaud, S. Grübel, S.-W. Huang, L. Huber, L. Patthey, Y.-D. Chuang, J. J. Turner, G. L. Dakovski, W.-S. Lee, M. P. Minitti, W. Schlotter, R. G. Moore, C. P. Hauri, S. M. Koohpayeh, V. Scagnoli, G. Ingold, S. L. Johnson, and U. Staub, Large-amplitude spin dynamics driven by a THz pulse in resonance with an electromagnon, Science **343**, 1333 (2014).

[7] S. Baierl, M. Hohenleutner, T. Kampfrath, A. K. Zvezdin, A. V. Kimel, R. Huber, and R. V. Mikhaylovskiy, Nonlinear spin control by terahertz-driven anisotropy fields, Nat. Photonics **10**, 715 (2016).

[8] E. Lesne, Y. Fu, S. Oyarzun, J. C. Rojas-Sanchez, D. C. Vaz, H. Naganuma, G. Sicoli, J.-P. Attane, M. Jamet, E. Jacquet, J.-M. George, A. Barthelemy, H. Jaffres, A. Fert, M. Bibes, and L. Vila, Highly efficient and tunable spin-to-charge conversion through Rashba coupling at oxide interfaces, Nat. Mater. **15**, 1261 (2016).

[9] Y. H. Ren, W. Lai, Z. Cevher, Y. Gong, and G. P. Zhang, Experimental demonstration of 55-fs spin canting in photoexcited iron nanoarrays, Appl. Phys. Lett. **110**, 082404 (2017).

[10] C. D. Stanciu, F. Hansteen, A. V. Kimel, A. Kirilyuk, A. Tsukamoto, A. Itoh, and Th. Rasing, All-Optical Magnetic Recording with Circularly Polarized Pight, Phys. Rev. Lett. **99**, 047601 (2007).

[11] S. Alebrand, A. Hassdenteufel, D. Steil, M. Cinchetti, and M. Aeschlimann, Interplay of heating and helicity in all-optical magnetization switching, Phys. Rev. B **85**, 092401 (2012).

[12] S. Alebrand, M. Gottwald, M. Hehn, D. Steil, M. Cinchetti, D. Lacour, E. E. Fullerton, M. Aeschlimann, and S. Mangin, Light-induced magnetization reversal of high-

anisotropy TbCo alloy films, Appl. Phys. Lett. **101**, 162408 (2012).

[13] S. Alebrand, U. Bierbrauer, M. Hehn, M. Gottwald, O. Schmitt, D. Steil, E. E. Fullerton, S. Mangin, M. Cinchetti, and M. Aeschlimann, Subpicosecond magnetization dynamics in TbCo alloys, Phys. Rev. B **89**, 144404 (2014).

[14] A. Hassdenteufel, B. Hebler, C. Schubert, A. Liebig, M. Teich, M. Helm, M. Aeschlimann, M. Albrecht, and R. Bratschitsch, Thermally assisted all-optical helicity-dependent magnetic switching in amorphous $Fe_{100-x}Tb_x$ alloy films, Adv. Mater. **25**, 3122 (2013).

[15] A. Hassdenteufel, J. Schmidt, C. Schubert, B. Hebler, M. Helm, M. Albrecht, and R. Bratschitsch, Low-remanence criterion for helicity-dependent all-optical magnetic switching in ferrimagnets, Phys. Rev. B **91**, 104431 (2015).

[16] T. A. Ostler *et al.*, Ultrafast heating as a sufficient stimulus for magnetization reversal in a ferrimagnet, Nat. Commun. **3**, 666 (2012).

[17] S. Mangin, M. Gottwald, C.-H. Lambert, D. Steil, V. Uhlir, L. Pang, M. Hehn, S. Alebrand, M. Cinchetti, G. Malinowski, Y. Fainman, M. Aeschlimann, and E. E. Fullerton, Engineered materials for all-optical helicity-dependent magnetic switching, Nat. Mater. **13**, 286 (2014).

[18] C.-H. Lambert, S. Mangin, B. S. D. Ch. S. Varaprasad, Y. K. Takahashi, M. Hehn, M. Cinchetti, G. Malinowski, K. Hono, Y. Fainman, M. Aeschlimann, and E. E. Fullerton, All-optical control of ferromagnetic thin films and nanostructures, Science **345**, 1337 (2014).

[19] K. Vahaplar, A. M. Kalashnikova, A. V. Kimel, D. Hinzke, U. Nowak, R. Chantrell, A. Tsukamoto, A. Itoh, A. Kirilyuk, and Th. Rasing, Ultrafast Path for Optical Magnetization Reversal via a Strongly Nonequilibrium State, Phys. Rev. Lett. **103**, 117201 (2009).

[20] V. N. Gridnev, Phenomenological theory for coherent magnon generation through impulsive stimulated Raman scattering, Phys. Rev. B **77**, 094426 (2008).

[21] D. Popova, A. Bringer, and S. Blügel, Theoretical investigation of the inverse Faraday effect via a stimulated Raman scattering process, Phys. Rev. B **85**, 094419 (2012).

[22] A. R. Khorsand, M. Savoini, A. Kirilyuk, A. V. Kimel, A. Tsukamoto, A. Itoh, and Th. Rasing, Role of Magnetic Circular Dichroism in All-Optical Magnetic Recording, Phys. Rev. Lett. **108**, 127205 (2012).

[23] J. H. Mentink, J. Hellsvik, D. V. Afanasiev, B. A. Ivanov, A. Kirilyuk, A. V. Kimel, O. Eriksson, M. I. Katsnelson, and Th. Rasing, Ultrafast Spin Dynamics in Multisublattice Magnets, Phys. Rev. Lett. **108**, 057202 (2012).

[24] A. Baral and H. C. Schneider, Magnetic switching dynamics due to ultrafast exchange scattering: A model study, Phys. Rev. B **91**, 100402(R) (2015).

[25] J. Gorchon, Y. Yang, and J. Bokor, Model for multi-shot all-thermal all-optical switching in ferromagnets, Phys. Rev. B **94**, 020409 (2016).

[26] V. N. Gridnev, Optical spin pumping and magnetization switching in ferromagnets, Phys. Rev. B **88**, 014405 (2013).

[27] T. D. Cornelissen, R. Cordoba, and B. Koopmans, Microscopic model for all optical switching in ferromagnets, Appl. Phys. Lett. **108**, 142405 (2016).

[28] G. P. Zhang, T. Latta, Z. Babyak, Y. H. Bai, and T. F. George, All-optical spin switching: A new frontier in femtomagnetism—A short review and a simple theory, Mod. Phys. Lett. B **30**, 16300052 (2016).

[29] D. A. Miller, Device requirements for optical interconnects to silicon chips, Proc. IEEE **97**, 1166 (2009).

[30] J.-Y. Chen, L. He, J.-P. Wang, and M. Li, All-optical switching of magnetic tunnel junctions with single subpicosecond laser pulses, Phys. Rev. Appl. **7**, 021001 (2017).

[31] P. Blaha, K. Schwarz, G. K. H. Madsen, D. Kvasnicka, and J. Luitz, *WIEN2K, An Augmented Plane Wave + Local Orbitals Program for Calculating Crystal Properties* (Technische Universität Wien, Vienna, 2001).

[32] G. P. Zhang, Y. H. Bai, and T. F. George, A new and simple model for magneto-optics uncovers an unexpected spin switching, Europhys. Lett. **112**, 27001 (2015).

[33] G. P. Zhang, Y. H. Bai, and T. F. George, Switching ferromagnetic spins by an ultrafast laser pulse: Emergence of giant optical spin-orbit torque, Europhys. Lett. **115**, 57003 (2016).

[34] P. M. Haney and M. D. Stiles, Current-Induced Torques in the Presence of Spin-Orbit Coupling, Phys. Rev. Lett. **105**, 126602 (2010).

[35] A. Manchon and S. Zhang, Theory of spin torque due to spin-orbit coupling, Phys. Rev. B **79**, 094422 (2009).

[36] R. John, M. Berritta, D. Hinzke, C. Müller, T. Santos, H. Ulrichs, P. Nieves, J. Walowski, R. Mondal, O. Chubykalo-Fesenko, J. McCord, P. M. Oppeneer, U. Nowak, and M. Münzenberg, Magnetization switching of FePt nanoparticle recording medium by femtosecond laser pulses, Sci. Rep. **7**, 4114 (2017).

[37] P. S. Pershan, J. P. van der Ziel, and L. D. Malmstrom, Theoretical discussion of the inverse Faraday effect, Raman scattering, and related phenomena, Phys. Rev. **143**, 574 (1966).

[38] G. P. Zhang and T. F. George, Total angular momentum conservation in laser-induced femtosecond magnetism, Phys. Rev. B **78**, 052407 (2008).

[39] R. Chimata, L. Isaeva, K. Kádas, A. Bergman, B. Sanyal, J. H. Mentink, M. I. Katsnelson, T. Rasing, A. Kirilyuk, A. Kimel, O. Eriksson, and M. Pereiro, All-thermal switching of amorphous Gd-Fe alloys: Analysis of structural properties and magnetization dynamics, Phys. Rev. B **92**, 094411 (2015).

[40] M. Berritta, R. Mondal, K. Carva, and P. M. Oppeneer, *Ab Initio* Theory of Coherent Laser-Induced Magnetization in Metals, Phys. Rev. Lett. **117**, 137203 (2016).

[41] K. Krieger, J. K. Dewhurst, P. Elliott, S. Sharma, and E. K. U. Gross, Laser-induced demagnetization at ultrashort time scales: Predictions of TDDFT, J. Chem. Theory Comput. **11**, 4870 (2015).

[42] P. Elliott, T. Müller, J. K. Dewhurst, S. Sharma, and E. K. U. Gross, Ultrafast laser-induced local magnetization dynamics in Heusler compounds, Sci. Rep. **6**, 38911 (2016).

[43] J. Simoni, M. Stamenova, and S. Sanvito, Ultrafast demagnetizing fields from first principles, Phys. Rev. B **95**, 024412 (2017).

[44] M. Stamenova, J. Simoni, and S. Sanvito, Role of spin-orbit interaction in the ultrafast demagnetization of small iron clusters, Phys. Rev. B **94**, 014423 (2016).

[45] G. P. Zhang, W. Hübner, G. Lefkidis, Y. Bai, and T. F. George, Paradigm of the time-resolved magneto-optical Kerr effect for femtosecond magnetism, Nat. Phys. **5**, 499 (2009).

[46] See Supplemental Material at http://link.aps.org/supplemental/10.1103/PhysRevB.96.134407 for the parameters used for each material. This includes the details about the lattice constants, electronic structure calculations, and untreated spin moment change for fcc Ni.

[47] M. S. El Hadri, M. Hehn, P. Pirro, C.-H. Lambert, G. Malinowski, E. E. Fullerton, and S. Mangin, Domain size criterion for the observation of all-optical helicity-dependent switching in magnetic thin films, Phys. Rev. B **94**, 064419 (2016).

[48] Peregrine Semiconductor, Peregrine Semiconductor reveals 60 GHz RF SOI switches (unpublished), http://www.psemi.com/newsroom/press-releases/381801-peregrine-semiconductor-reveals-60-ghz-rf-soi-switches.

[49] K. F. Lee, X. Ding, T. J. Hammond, M. E. Fermann, G. Vampa, and P. B. Corkum, Harmonic generation in solids with direct fiber laser pumping, Opt. Lett. **42**, 1113 (2017).

[50] R. P. Williams, S. G. Alcock, P. B. Howes, and C. L. Nicklin, Growth, morphology, and structure of a monolayer thick $GdFe_2$ surface alloy, Phys. Rev. B **94**, 075419 (2016).